Energy & Environmental Science

Cite this: *Energy Environ. Sci.*, 2011, **4**, 3414

www.rsc.org/ees

PAPER

Origin of efficiency enhancement in Nb_2O_5 coated titanium dioxide nanorod based dye sensitized solar cells†‡

Eva Barea,*[a] Xueqing Xu,[ab] Victoria González-Pedro,[a] Teresa Ripollés-Sanchis,[a] Francisco Fabregat-Santiago*[a] and Juan Bisquert[a]

Received 20th February 2011, Accepted 22nd March 2011
DOI: 10.1039/c1ee01193f

Ordered one-dimensional metal oxides are considered promising architectures for dye-sensitized solar cells (DSC). Here we explore the properties determining the photovoltaic performance of DSC based on titanium dioxide nanorods prepared by a hydrothermal method. Ultrathin conformal coating with other oxides such as Al_2O_3 or Nb_2O_5 has been widely used in the literature to improve the conversion efficiency. Usually the effects attributed to the coating are either to prevent recombination by barrier effect or to change the position of titanium dioxide conduction band. Here we show that coating TiO_2 nanorods with Nb_2O_5 increases the photocurrent and conversion efficiency of the DSC. However, impedance spectroscopy results indicate that neither recombination is reduced by the coating nor the conduction band position is moved. The improvement in the performance of the cell has been attributed to an enhancement in the charge injection efficiency promoted by Nb_2O_5.

Introduction

Dye solar cells (DSCs)[1] are a relatively low cost photovoltaic technology that may be used in new applications such as building integrated systems as windows or façades to produce electricity. DSCs also have the potential to compete with other photovoltaic technologies in the search for environmentally clean sources of electrical energy. DSCs have yielded to date up to 11.3% solar-to-electric power conversion efficiencies under 1 sun illumination,[2] and there is strong research in the field to push this value up with very promising results.

The performance of DSC devices is mainly determined by the type of sensitizer, the electrolyte and the properties of the porous semiconducting electrodes that are used in their fabrication.[3,4] The electron collecting electrode is typically a 12 μm thick film composed of two different layers of TiO_2 nanoparticles, a transparent one (~8 μm) and a light scattering layer (~4 μm) creating an interconnected semiconductor network for electron collection towards the contact.[5,6] The structure of these electrodes presents a large surface area that enables abundant dye upload on the surface to maximize the amount of photogenerated charge. In addition to efficient light harvesting, to obtain good collection efficiency it is needed that the titanium dioxide nanoparticles have a large diffusion length.[7,8]

Over the past several years highly ordered TiO_2 nanostructures such as nanowires (*nw*), nanotubes (*nt*) or nanorods (*nr*) have become the focus of considerable interest since they possess unique properties suitable for both solid and liquid hole conductor DSC applications. They keep a large specific surface

[a]*Grup de Dispositius Fotovoltaics i Optoelectrònics, Departament de Física. Universitat Jaume I, Castelló, Spain. E-mail: fran.fabregat@fca.uji.es; barea@fca.uji.es; Tel: 12071*
[b]*Guangzhou Institute of Energy Conversion, Renewable Energy and Gas Hydrate Key Laboratory of Chinese Academy of Sciences, Guangzhou, 510640, China*

† This article was submitted as part of an issue highlighting papers from the International Conference on Ordered 1-Dimensional Nanostructures for Photovoltaics, held in September 2010.

‡ Electronic supplementary information (ESI) available. See DOI: 10.1039/c1ee01193f

Broader context

Dye solar cells are one of the technologies proposed for cutting down the price of photovoltaic solar energy. Nano-ordered structures such as nanorods and nanotubes are some of the latest configurations proposed to increase the efficiency in this device and improve charge collection. Through advanced electrical models, this paper studies the mechanisms that determine the photovoltaic performance of dye solar cells made from bare and Nb_2O_5 coated TiO_2 nanorods. It clarifies which is the origin of the improvement provided by the addition of the Nb_2O_5 discarding many of the ideas typically argued to justify the improvements attained with this configuration.

that allows similar dye adsorption as in the nanoparticles, while the continuous and ordered structure offers both, direct conduction pathways for the extraction of photogenerated charges and a more suitable structure for the penetration of the solid hole conductor. The uninterrupted pathways are expected to improve the electron transport properties and thus the charge collection.[9–12]

Several fabrication routes including anodic oxidation,[13,14] electrochemical lithography,[15] photoelectrochemical etching,[16] sol–gel,[17] hydrothermal synthesis,[18–21] and template synthesis[22,23] have been used to prepare these ordered TiO_2 nanostructures. In some cases the preparation of titanium dioxide *nt* has been successful in improving the photocurrent and conversion efficiency of DSCs.[24,25]

Further improvement has been reported after the introduction of transition metals like Ta in titanium dioxide *nt* with an enhancement on the photovoltage of the DSCs.[10] Other strategies consist on modifying the surface of the nanostructures with metal oxides like Al_2O_3, Nb_2O_5, ZnO or $CaCO_3$, as it has previously been done for nanocolloidal TiO_2 electrodes.[24,26,27] All these works reported improvements in the short circuit current (j_{sc}) and, depending on the treatment, the open circuit potential (V_{oc}), enhancing the overall conversion efficiency of the DSC, which has been attributed to several factors such as the blocking of surface recombination or shifts in the conduction band edge.

In the particular case of Nb_2O_5, this material has shown good absorption of Ru dyes and a conduction band which is 100 mV above the conduction band TiO_2.[28] The combined effect of good dye loading and the energy gradient created by the surface coating should help in charge separation and collection.[29] Enhanced photocurrent was found by Zaban in nanocoloidal TiO_2 coated with Nb_2O_5[27,29] which also yielded an increase in V_{oc}, and by Feng in TiO_2 coated nanorods,[18] in this case without an increase in V_{oc}.

In this paper we analyze the parameters that determine the photovoltaic performance of DSCs based on highly ordered transparent TiO_2 *nr* using N719 dye as sensitizer. We study the electrical and operational differences between DSC made with *nr* electrodes of pure TiO_2 and *nr* coated with a thin layer of Nb_2O_5. We discuss and determine the origin of the increase of the overall conversion efficiency from 4.18 to 5.24% and the j_{sc} from 9.70 to 12.2 mA cm^{-12}.

Experimental

Nanorod synthesis and niobium oxide coating

Highly ordered transparent titanium dioxide *nr* arrays were prepared by a hydrothermal method similar to a previously reported route.[18] Well cleaned glass substrates coated with fluorine doped tin oxide (FTO) were dip-coated in a titanium tetrachloride 40 mM solution for 30 min at 70 °C, then rinsed with water and ethanol and subsequently heated at 570 °C for 10 min to obtain a layer of TiO_2. The as-treated FTO substrates were then loaded into a sealed Teflon lined stainless steel autoclave containing 30 mL toluene and 5 mL hydrochloride acid (35%). To this mixture, 5 mL of a 1 M solution of $TiCl_4$ in toluene, 5 g of titanium(IV) butoxide and finally, 20 mL of toluene were added drop by drop. The reaction temperature was 180 °C for 18 h. After the reaction was completed, the autoclave was cooled down fast until room temperature to stop the reaction. The resulting *nr*s were washed with ethanol and heated at 450 °C for 30 min in air to remove possible organic residual species.

In order to prepare niobium coated *nr*, the as synthesized electrodes were treated with niobium(v) chloride (99.9%) according to previous work by Zaban.[27] The TiO_2 *nr* were deep in 5 mM solution of $NbCl_5$ in dry ethanol for 30 s under nitrogen atmosphere, rinsed with ethanol and sintered at 500 °C 30 min.

DSC fabrication

To prepare the DSCs, the *nr* electrodes were immersed into N719 dye solution (0.3 mM *tert*-butanol/acetonitrile) overnight. After adsorption of the dye, the electrodes were rinsed in *tert*-butanol/acetonitrile. The solar cells were assembled with a counter electrode, thermally platinized FTO, using a thermoplastic frame of Surlyn 25 μm thick. The redox electrolyte (0.6 M 1-butyl-3-methylimidazolium iodide (BMII), 0.1 M LiI (99,9%), 0.01 M I_2 (99,9%), 0.1 M guanidinium thiocyanate and 0.4 M 4-*tert*-butylpiridine in acetonitrile : valeronitrile 85 : 15) was then introduced through a hole drilled in the counter-electrode that was sealed afterwards. The resulting solar cells had an active area of 0.4 cm^2.

Sample charecterization

Microstructural examination was carried out by using a scanning electron microscope (SEM) model JSM-7000F (Jeol) equipped with an INCA 400 (Oxford) EDS analyzer and a transmission electron microscope (TEM) model JEM 2100 (Jeol) equipped with INCA X-sight a EDX analyzer (Oxford).

DSC were characterized by current–voltage (j–V) and impedance spectroscopy (IS) analysis using a 0.25 cm^2 mask. The measurements were carried out using with a PG-STAT30 potentiostat (Autolab) and a solar simulator equipped with a 1000 W ozone-free Xenon lamp and AM 1.5 G filter (Oriel), where the light intensity was adjusted with an NREL-calibrated Si solar cell with a KG-5 filter to 1 sunlight intensity (100 $mWcm^{-2}$). Impedance spectroscopy measurements were done from 0 to 0.8 V at 50 mV steps, using a range of frequencies between 1 MHz and 10 mHZ.

Differences in dye uptake were measured through the transmittance of the resulting solution obtained after soaking the film in 0.1 M *tert*-butylammonium hydroxide in acetonitrile.[30]

Results and discussion

Nanorods characterization

SEM measurements of transversal cross-sections of unsensitized photoanodes are shown in Fig. 1(a) to (c). Fig. 1(a) presents a view of the transparent titanium dioxide *nr* obtained by hydrothermal synthesis. It may be observed that a highly uniform and densely packed array of nanorods has grown perpendicular from the substrate to an approximate length of 3.5 μm with an average diameter of 37 nm, as can be seen from the cross-section view of Fig. 1(b). For Nb_2O_5 coated *nr*, Fig. 1

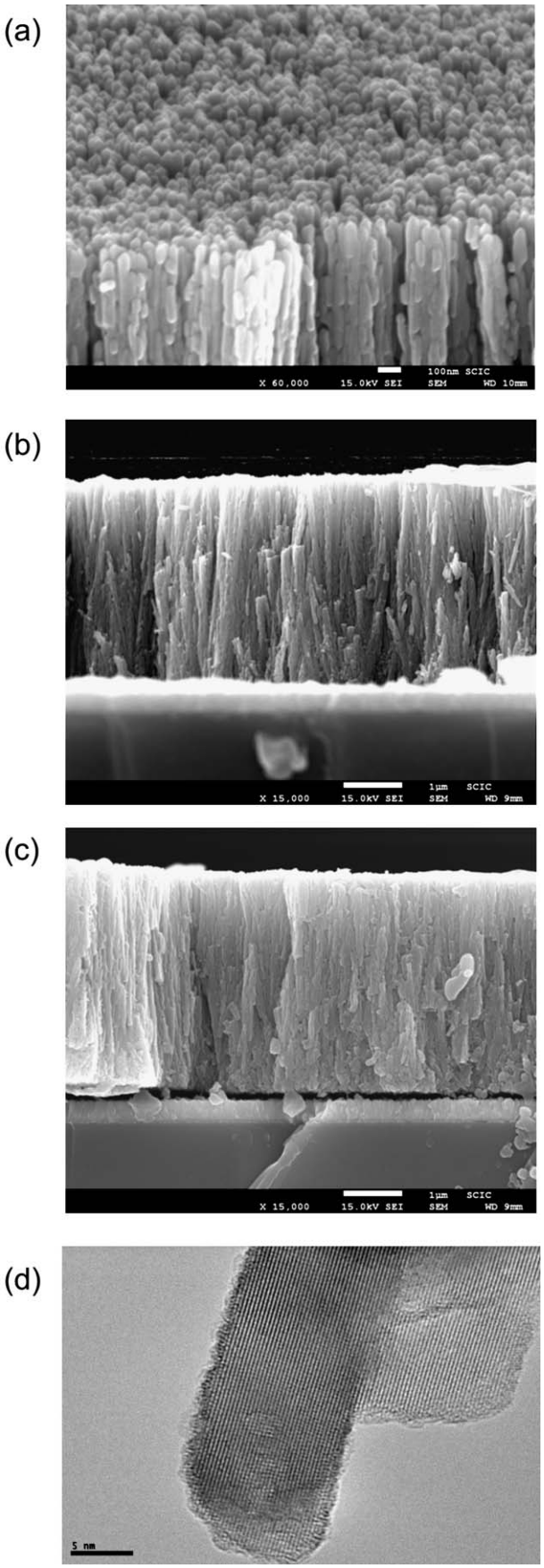

(c), no changes were observed neither in thickness nor in length of the rods.

TEM measurements to Nb_2O_5 coated nanorods, Fig. 1(d), showed large crystals of TiO_2 with amorphous borders where the Nb_2O_5 coating is seated. Interplanar distances of 3.2 Å corresponding to the plane (110) of the TiO_2 rutile phase, which matches previous reports.[18] EDX analysis showed that Nb is uniformly distributed along the composite, although we have observed some local non-uniformity along the coating. Thus the amorphous layers on the top of the nanorods had a maximum thickness of 10 Å, whereas other regions had the thickness dropped down to around 3 Å.

Solar cell study

Fig. 2 compares the *j–V* curves (lines) for DSCs sensitized with N719 based on TiO_2 *nr* and Nb_2O_5-coated TiO_2 *nr*. The parameters that describe the DSC performance are summarized in Table 1. For the Nb_2O_5-coated sample the photocurrent increases nearly 26% (from 9.70 to 12.2 mA cm^{-2}) keeping the value of V_{oc} nearly constant, which implies a 25% enhancement in the performance of the Nb-coated titanium dioxide *nr* based DSC (5.24%) with respect to a normal titanium dioxide *nr* based DSC (4.18%). To ensure the reproducibility and consistency of the results, experiments were repeated 3 times, building fresh solar cells each time, and determining *j–V* curves for all the samples. The stability of the DSC has been checked in all cases after IS measurements under illumination, always obtaining the same results as the fresh *j–V* curve. Therefore, Fig. 2 and the obtained parameters summarized in Table 1 are highly representative of the behaviour of the solar cells fabricated.

The impedance spectra of the complete DSCs were analyzed by making use of the transmission line model described elsewhere.[4,31,32] Fig. 3 shows a characteristic spectrum that realizes well the transmission line model and allows to obtain the main electrical parameters that determine the behavior of the cell: recombination resistance (R_{rec}), the cell capacitance (C), transport resistance (R_{tr}) and the other contributions to the series resistance (R_s). The data obtained are used to elucidate the differences in the behaviour of the bare and the Nb-coated cells.

The analysis of recombination resistance over parameters such as lifetime presents the advantage that it eliminates the dependence on capacitances associated to charge accumulation in the device. Therefore it provides a more direct measurement of the recombination process.[8,33]

At first sight, the values of the recombination resistance represented *vs.* the applied potential (V_{ap}) in Fig. 4(a), are equal for most of the potentials, both in bare and Nb-coated samples. However for a proper comparison it is necessary to remove the effect of series resistance R_s in the voltage scale. Subtracting the

Fig. 1 SEM images of a vertically oriented self-organized TiO_2 nanorods array grown on FTO substrate. (a) Top-cross view images of TiO_2 *nr*, (b) cross-section image of the same array, and (c) cross-section image of Nb_2O_5 coated TiO_2 *nr*. (d) TEM image of the end of Nb_2O_5 coated TiO_2 *nr* presenting the rutile crystal surrounded by an amorphous border which includes Nb_2O_5.

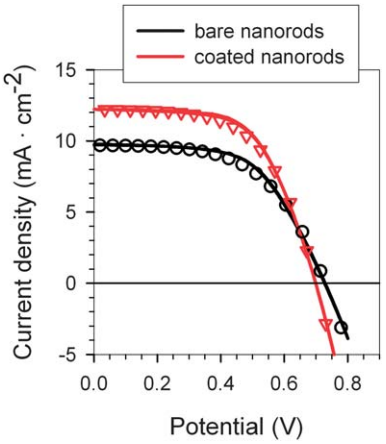

Fig. 2 Current density–potential curves for nanorod based DSCs, at 1 sunlight intensity. The lines represent the *j–V* curves, the dots represent the simulated *j–V* curves from impedance data.

Table 1 Photovoltaic performance of DSCs using TiO_2 nanorods and TiO_2 nanorods coated with Nb_2O_5. Both DSCs were sensitized by N719 dye. j_{sc} is the short circuit photocurrent density, V_{oc} the open-circuit voltage, *FF* the fill factor, η the power conversion efficiency, and finally, *internal FF* and *internal* η are the corrected values of FF and η after suppressing the series resistance potential drop

TiO_2 nanorod	V_{oc}(V)	j_{sc} (mA cm^{-2})	FF	η (%)	internal FF	internal η (%)
bare	0.73	9.70	0.59	4.18	0.62	4.39
coated	0.70	12.2	0.61	5.24	0.64	5.46

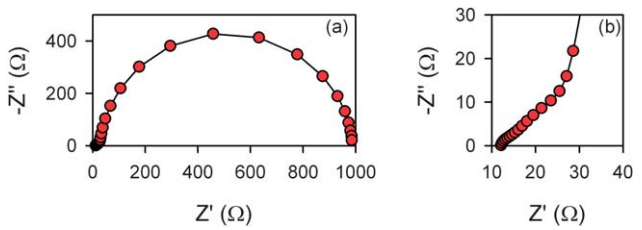

Fig. 3 (a) Impedance spectra for a DSC made from bare TiO_2 nanorods, at 1 sunlight intensity and 0.45 V. (b) Zoom-in of (a) showing at high frequencies the diffusive behavior of the electrons in the DSC, characteristic of the transmission line model.

effect of the series resistance, we may define a Fermi level voltage $V_F = V_{ap} - jR_s$.[34]

Using this corrected potential, the recombination resistance may be written as

$$R_{rec} = R_0 \exp\left[-\beta \frac{qV_F}{k_B T}\right], \quad (1)$$

with R_0 a constant indicating the onset of recombination, β the recombination parameter (also named charge transfer coefficient) governing the non-linear recombination, q the charge of the electron, k_B the Boltzmann constant and T the temperature. Now it is possible to analyze the differences found in Fig. 4(c) between both samples: the value of R_{rec} for the coated TiO_2

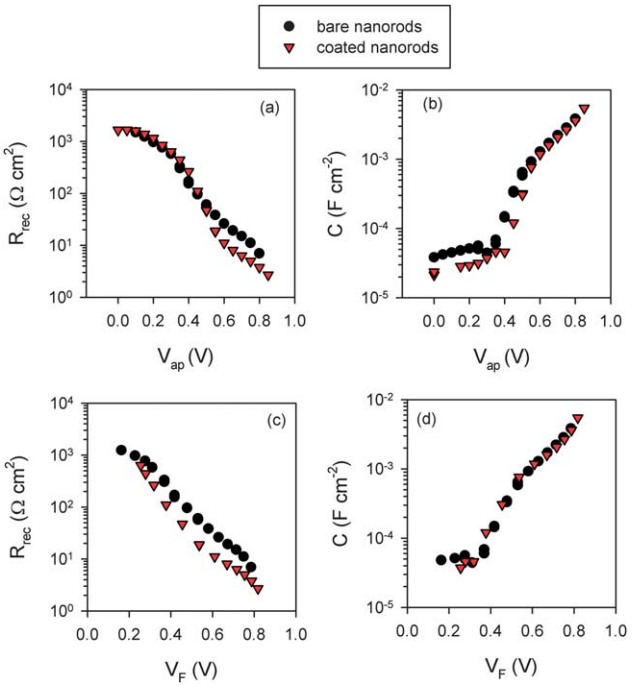

Fig. 4 Recombination resistance and chemical capacitance obtained from impedance analysis at 1 sun illumination of bare and Nb_2O_5 coated TiO_2 nanorods. Sections (a) and (b) are plotted with respect to the applied voltage in the solar cell. Sections (c) and (d) are plotted with respect to the Fermi level voltage (without the effect of series resistance) defined as $V_F = V_{ap} - jR_s$.

nanorods is smaller (R_0 = 5000 Ω cm^2) than for the uncoated (R_0 = 7200 Ω cm^2) sample. This result indicates that the coating is *not* forming a blocking layer at the surface of the TiO_2 able to reduce recombination losses. The slope of R_{rec} is slightly higher for the coated TiO_2, providing a recombination parameter[4,7] β = 0.27 *vs.* β = 0.23 in the case of the bare nanorods (see the ESI for more details).‡ The value of β is around half of the typical value associated with charge transfer from TiO_2 anatase colloids to the I_3^- in the electrolyte.[7,35,36] This difference could be associated with the rutile phase of the nanorods. Although Nb_2O_5 coating does not increase the absolute value of R_{rec}, it produces a rise in β.

After correction of the potentials, the capacitance of the two studied samples presents nearly the same values, Fig. 4(d). At voltages above V_F = 0.4 V we observe the characteristic behaviour of the chemical capacitance (C_μ, see ESI‡): an exponential rise with increasing potentials. As $C_\mu = q^2 g(E_F)$, the distribution of electron trap states below the conduction band of TiO_2 follows the expression[37]

$$g(E_F) = \frac{N_c}{k_B T} \exp\left[\frac{E_{Fn} - E_C}{k_B T_0}\right] \quad (2)$$

with the parameter that describes the distribution of traps taking the value T_0 = 1100 K ($\alpha = T/T_0$ = 0.25). Data from Fig. 4(d) show that $g(E_F)$ is dominated by TiO_2, with no contribution given by the coating.

The coincidence in the values of the capacitance found also indicates that the conduction band edge in the TiO_2 has not been altered by the addition of the Nb_2O_5. This result is corroborated

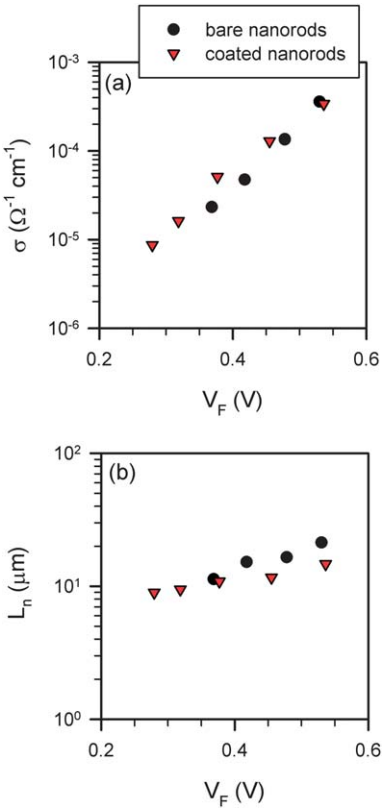

Fig. 5 (a) Conductivity and (b) diffusion length of DSC based on bare and Nb_2O_5 coated TiO_2 nanorods *vs.* the Fermi level voltage at 1 sun illumination.

by the good match found for the electron conductivity, of the different nanorods shown in Fig. 5(a), which is calculated from

$$\sigma = \frac{L}{R_{tr} S(1-p)} \tag{3}$$

with L being the nanorod thickness, S the surface and p the porosity of the film. These results indicate that the increased photocurrent of Nb-coated DSC may not be associated with a downward shift of the band-edge of the semiconductor.[31,28]

Transport and recombination resistances allow us to calculate the small perturbation diffusion length of electrons *via* the expression[38,39]

$$L_n = L\sqrt{\frac{R_{rec}}{R_{tr}}} \tag{4}$$

As shown in Fig. 5(b), L_n is slightly lower for the coated film due to the higher recombination rate in this sample. In any case the diffusion length is about 4 times larger than the rod length ensuring that the injected charge is efficiently collected.

In general, the improvement of DSC performance with ultrathin conformal coating in nanostructured films is either associated with the suppression of recombination[26] or with the shift of the conduction band. However our results show that none of these effects may explain the increase in j_{sc} and the efficiency produced by addition of the Nb_2O_5 to the TiO_2 *nr*. The IPCE of Fig. 6 suggests that the improvement of the modified TiO_2 *nr* DSC is due to an increase in the injection yield from the dye.

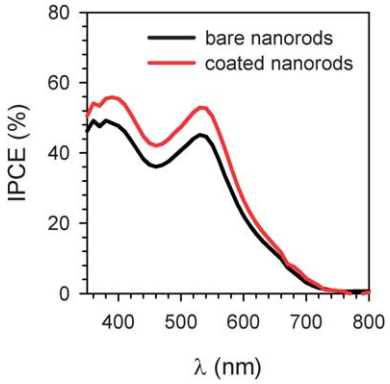

Fig. 6 External quantum efficiency plots of DSCs based on bare and Nb_2O_5 coated TiO_2 nanorods.

Dye desorption measurements indicate that the difference in the dye uptake is only 4%, therefore the main origin of the largely improved j_{sc} may only be due to an increased charge injection efficiency of the dye into the rutile nanorods, facilitated by the presence of niobium oxide coating. Future work will be devoted to thorough exploration of this enhanced injection yield.

Recombination resistance, photocurrent and *j–V* curves

One of the reasons for larger V_{oc} in DSC is attributed to upward shifts in the conduction band-edge position of TiO_2.[40] However, as we have stated above, here the conduction band position in the TiO_2 is unmodified by the coating, therefore V_{oc} is determined by both R_{rec} and j_{sc}.

The relation between recombination resistance and recombination current is given by[4]

$$R_{rec} = \left(\frac{\partial j_{rec}}{\partial V_F}\right)^{-1} \tag{5}$$

In the case where the series resistance is zero, the current from the *j–V* curve may be obtained from

$$j = j_{SC} - \int_0^V \frac{dV_F}{R_{rec}} \tag{6}$$

which, using eqn (1) yields the diode equation typically used in p-n junction solar cells[41]

$$j = j_{sc} - j_0\left[\exp\left(\beta\frac{qV_F}{k_B T}\right) - 1\right] \tag{7}$$

with $\beta = 1/m$ as the inverse of the ideality factor and

$$j_0 = \frac{k_B T}{q\beta R_0} \tag{8}$$

as the reverse current.

The larger value of R_0 (lower j_0), together with the smaller β provide the greater V_{oc} observed for the bare TiO_2 *nr*. The coated sample could not compensate its poorer R_{rec} to reach similar or larger V_{oc} (see ESI for more details).‡

This analysis allows calculating the internal (maximum) efficiencies and FF (see Table 1) that could be achieved if the series

resistance was completely removed from the solar cell. Here a 5% rise was obtained for these parameters.

When considering the total resistance of the device $R_{Tot} = R_{rec} + R_s + R_{tr}/3$, it is possible to regenerate the j–V curve shown in Fig. 1 through the equation:

$$j = j_{SC} - \int_0^V \frac{dV}{R_{Tot}} \quad (9)$$

As the dots in Fig. 1 show, an excellent match was found between the data, confirming the intrinsic relationship between the impedance parameters and the dc characteristics of the cell.

Finally, the increase in the FF observed in Table 1, for the coated *nr* can be explained in terms of these electrical measurements. The sample with Nb_2O_5 coating presents both a larger β and a smaller series resistance (on average 20 Ω *vs.* 25 Ω for bare TiO_2) and both effects contribute to the rise in the FF.[4]

Conclusions

An increase of 25% in energy conversion efficiency was observed in titanium dioxide nanorod based DSC by application of thin Nb_2O_5 coating on the surface. The main factor contributing to the improvement of the performance is the enhancement of the electron injection yield. Some usual factors contributing to the improvement such as an increase on the diffusion length, the formation of a surface recombination blockage with the coating or a shift in the conduction band, have been discarded by experimental measurements.

Acknowledgements

We are thankful for financial support from Ministerio de Cíencia e Innovación under Projects HOPE CSD2007-00007 and MAT 2010-19827, Generalitat Valenciana under Project PROMETEO/2009/058 and Programa de Mobilidad del Personal Investigador de Bancaixa. Servei Central d'Instrumentació Científica of Universitat Jaume I is acknowledged for the SEM and TEM measurements, and Sixto Gimenez for fruitful discussions.

References

1 B. O'Regan and M. Gratzel, *Nature*, 1991, **353**, 737–740.
2 F. Gao, Y. Wang, D. Shi, J. Zhang, M. Wang, X. Jing, R. Humphrey-Baker, P. Wang, S. M. Zakeeruddin and M. Gratzel, *J. Am. Chem. Soc.*, 2008, **130**, 10720.
3 M. Gratzel, *Inorg. Chem.*, 2005, **44**, 6841–6851.
4 F. Fabregat-Santiago, J. Bisquert, E. Palomares, L. Otero, D. Kuang, S. M. Zakeeruddin and M. Grätzel, *J. Phys. Chem. C*, 2007, **111**, 6550–6560.
5 S. Ito, Y. Yamada, M. Kuze, K. Tabata and T. Yashima, *J. Mater. Sci.*, 2004, **39**, 5853–5856.
6 M. Gratzel, *J. Photochem. Photobiol., A*, 2004, **168**, 235.
7 Q. Wang, S. Ito, M. Grätzel, F. Fabregat-Santiago, I. Mora-Seró, J. Bisquert, T. Bessho and H. Imai, *J. Phys. Chem. B*, 2006, **110**, 19406–19411.
8 F. Fabregat-Santiago, J. Bisquert, L. Cevey, P. Chen, M. Wang, S. M. Zakeeruddin and M. Grätzel, *J. Am. Chem. Soc.*, 2009, **131**, 558–562.
9 A. Hagfeldt and M. Gratzel, *Acc. Chem. Res.*, 2000, **33**, 269–277.
10 X. Feng, F. Shankar, M. Paulose and C. A. Grimes, *Angew. Chem., Int. Ed.*, 2009, **48**, 8095–8098.
11 G. K. Mor, J. Basham, M. Paulose, S. Kim, O. K. Varghese, A. Vaish, S. Yoriya and C. A. Grimes, *Nano Lett.*, 2010, **10**, 2387–2394.
12 D. C. Olson, S. E. Shaheen, R. T. Collins and D. S. Ginley, *J. Phys. Chem. C*, 2008, **112**, 9544–9547.
13 D. W. Gong, C. A. Grimes and O. K. Varghese, *J. Mater. Res.*, 2011, **16**, 3331–334.
14 J. Choi, R. B. Wehrspohn, F. Lee and U. Göele, *Electrochim. Acta*, 2004, **49**, 2645–2652.
15 S. Z. Chu, S. Inoue, K. Wada, S. Hishita and K. Kurashima, *J. Electrochem. Soc.*, 2005, **152**, B116–B124.
16 H. Masuda, K. Kanezawa, M. Nakao, A. Yokoo, T. Tamamura, T. Sugiura, H. Minoura and K. Nishio, *Adv. Mater.*, 2003, **15**, 159–161.
17 J. E. Wijnhoven, *Science*, 1998, **281**, 802–804.
18 X. Feng, K. Shankar, O. K. Varghese, M. Paulose, T. J. Latempa and C. A. Grimes, *Nano Lett.*, 2008, **8**, 3781–3786.
19 W. Z. Wang, O. K. Varghese, M. Paulose and C. A. Grimes, *J. Mater. Res.*, 2004, **19**, 417–422.
20 P. L. Chen, C. T. Kuo and F. M. Pan, *Appl. Phys. Lett.*, 2004, **84**, 3888–3890.
21 D. V. Bavykin, V. N. Parmon, A. A. Lapkin and F. C. Walsh, *Journal of Material Chemistry*, 2004, **14**, 3370–3377.
22 P. Hoyer, *Langmuir*, 1996, **12**, 1411–1413.
23 X. H. Li, W. M. Liu and H. L. Li, *Appl. Phys. A: Mater. Sci. Process.*, 2003, **80**, 317–320.
24 Z. S. Wang, M. Yanagida, K. Sayama and H. Sugihara, *Chem. Mater.*, 2006, **18**, 2912.
25 K. E. Kim, S. R. Jang, J. Park, R. Vittal and K. J. Kim, *Sol. Energy Mater. Sol. Cells*, 2007, **91**, 366.
26 F. Fabregat-Santiago, J. García-Cañadas, E. Palomares, J. N. Clifford, S. A. Haque, J. R. Durrant, G. Garcia-Belmonte and J. Bisquert, *J. Appl. Phys.*, 2004, **96**, 6903–6907.
27 S. G. Chen, S. Chappel, Y. Diamant and A. Zaban, *Chem. Mater.*, 2001, **13**, 4629–4634.
28 K. Sayama, M. Sugino, H. Sugihara, Y. Abe and H. Arakawa, *Chem. Lett.*, 1998, 753.
29 A. Zaban, S. G. Chen, S. Chappel and B. A. Gregg, *Chem. Commun.*, 2000, 2231–2232.
30 S. Ito, T. N. Murakami, P. Comte, P. Liska, C. Grätzel, M. K. Nazeeruddin and M. Grätzel, *Thin Solid Films*, 2008, **516**, 4613–4619.
31 F. Fabregat-Santiago, J. Bisquert, G. Garcia-Belmonte, G. Boschloo and A. Hagfeldt, *Sol. Energy Mater. Sol. Cells*, 2005, **87**, 117–131.
32 E. M. Barea, J. Ortiz, F. J. Payá, F. Fernández-Lázaro, F. Fabregat-Santiago, S.-S.A. and J. Bisquert, *Energy Environ. Sci.*, 2010, 3.
33 J. Bisquert and F. Fabregat-Santiago, in *Dye-sensitized Solar Cells*, ed. K. Kalyanasundaram, EPFL Press, Lausanne. Distributed by CRC Press, Boca Raton, 2010.
34 E. M. Barea, C. Zafer, B. Gultein, B. Aydin, S. Koyuncu, S. Icli, F. Fabregat-Santiago and J. Bisquert, *J. Phys. Chem. C*, 2010, **114**, 19840–19848.
35 M. Wang, P. Chen, R. Humphry-Baker, S. M. Zakeeruddin and M. Gratzel, *ChemPhysChem*, 2009, **10**, 290–299.
36 J. Liu, R. Li, X. Si, D. Zhou, Y. Shi, Y. Wang, X. Jing and P. Wang, *Energy Environ. Sci.*, 2010, **3**, 1924–1928.
37 J. Bisquert, *Phys. Chem. Chem. Phys.*, 2003, **5**, 5360.
38 J. Bisquert, *J. Phys. Chem. B*, 2002, **106**, 325–333.
39 J. Bisquert and I. Mora-Seró, *J. Phys. Chem. Lett.*, 2010, **1**, 450–456.
40 Y. Liu, A. Hagfeldt, X.-R. Xiao and S.-E. Lindquist, *Sol. Energy Mater. Sol. Cells*, 1998, **55**, 267–281.
41 S. M. Sze, *Physics of Semiconductor Devices*, John Wiley and Sons, New York, 1981.